Low permeability measurement on crushed rock: insights

Sandra Profice[1,*], and *Roland* Lenormand[2]

[1]TOTAL CSTJF, avenue Larribau, 64018 Pau Cedex, France
[2]CYDAREX, 31 avenue Gabriel Péri, 92500 Rueil-Malmaison, France

Abstract. The Gas Research Institute (GRI) method enabling permeability measurement on crushed samples or drill cuttings was proposed by Luffel *et al.* in the early 90's. This paper presents the study led by Cydarex and Total to (i) Analyze the validity of permeabilities determined with GRI methods applied in the industry (ii) Collect information about these methods (iii) Explain the discrepancies between the results collected for similar rocks. Three materials were selected: one homogeneous outcrop rock and two reservoir rocks having absolute permeabilities ranging from 1 to 50 nD and anisotropy ratios varying from 1 to 3. For each rock, the permeabilities delivered by three commercial laboratories having their own GRI techniques were compared to the permeabilities we derived with the DarcyPress and Step Decay techniques. In addition to use different methods, the companies worked on diverse samples going from the plug of a few centimeters to the pack of millimetric particles. It was highlighted that the dispersion in the permeability data increases when the sample characteristic length decreases. To better understand the observations, the results were analyzed considering many things: literature, laboratories' crushed samples, laboratories' data and information, permeability values from GRI tests we undertook, numerical simulations…

1 Introduction

In the early 90's, Luffel *et al.* [1] developed the method of permeability measurement on crushed rock or drill cuttings, named Gas Research Institute (GRI) method. In this method, a pressure pulse is emitted at the surface of the particles and the signal due to fluid flow in the sample pore network is recorded over time. As a consequence, a GRI test is nothing more than a pycnometry test. The GRI or pycnometry device generally found in the industry is schematically represented on Figure 1.

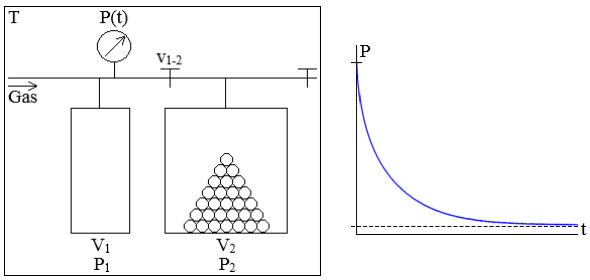

Fig. 1. GRI or pycnometry device and recorded pressure signal

The sample is in a chamber of volume V_2 connected to a chamber of volume V_1 via a valve $v_{1\text{-}2}$. Initially, the valve $v_{1\text{-}2}$ is closed and the pressure in the dead volume of the chamber V_2 as well as the pressure in the sample pore volume are at P_2. The test starts with the pressurization of the chamber V_1 at a pressure P_1 higher than the pressure P_2. At time t=0, the valve $v_{1\text{-}2}$ is opened and the recording of the pressure transient P(t) is triggered simultaneously. The temperature T of the system is kept constant either by regulating the laboratory temperature or by placing it in a temperature-controlled oven.

The option to work on rock particles is attractive as the test duration is considerably shortened by the increase of the medium exchange area with the invading fluid and the decrease of the medium characteristic penetration depth [2]. Moreover, this option should also drastically reduce the test cost considering that only a few grams of cuttings recovered while drilling are theoretically enough. Another argument defended by Luffel *et al.* [1] is the elimination during crushing of the coring-induced microfractures. The authors maintain that the microfractures remain open even when confining the core sample, which creates a bias in the estimated matrix permeability. However, the fact that tests under realistic confining pressures are not possible with the GRI method is as problematic as the existence of microfractures, low permeable media being very sensitive to stress [3]. Recent papers from the literature pointed out additional issues. Passey *et al.* [4] observed a significant dispersion of the permeabilities determined for identical samples by different commercial laboratories having their own devices, experimental procedures and interpretative models. The discrepancies between the values reached up to several decades. The reasons of these discrepancies are not discussed in the paper maybe because the authors did not have the elements needed to analyze the results.

Among the elements which could be responsible for the discrepancies, the rock pore network alteration during crushing could be a possibility. In his experimental work on the GRI method, Tinni [5] demonstrated the influence

*Corresponding author: sandra.profice@total.com

of the mean particle size on the estimated permeability. He noticed permeability increases of more than two orders of magnitude in the worst cases, when the mean particle diameter square increases from 0.1 to 100 mm^2. Tinni [5] assessed the influence of several other parameters on the permeability: amount of rock particles in the chamber V_2, initial pressure in the chamber V_1, gas nature, initial free water content in the particles and flushing of the system with the test gas before analysis. He highlighted that, in addition to the particle size, the sample pore volume and the pressure level act considerably on the permeability.

The permeability is also possibly affected by the rock anisotropy [3] and the thermal perturbations occurring at early times after opening the valve $v_{1\text{-}2}$ [2, 6]. A GRI test does not give a directional permeability, the gas invading the rock particles in the three space directions. This means that, for anisotropic samples such as laminated shales for instance, the permeability resulting from a GRI test is a combination of the permeabilities in the three directions. The thermal effects are of two types [6]. The first effect appears when the gas quickly expands from the chamber V_1 to the chamber V_2. The second one, known as Joules-Thomson effect, originates from the slow expansion of the gas through the porous medium. Both effects create biases in the pressure values recorded at early times.

The last element impacting permeability estimation is the model used to interpret P(t). Few models are reported in the literature and the consequences of the simplifying assumptions made, when modeling the physical problem, are rarely easy to evaluate. The most usual simplification regards the sample geometry. The sample consists of rock particles with arbitrary shapes and variable sizes covering an interval depending on the way it was prepared. While Luffel *et al.* [2] assimilated the sample to a monodisperse pack of cylinders, many other authors who focused later on the GRI method assimilated it to a monodisperse pack of spheres [2, 5, 7].

We studied the GRI methods used routinely by three commercial laboratories. The first objective was to check the coherence between the permeabilities delivered by the laboratories and the permeabilities we measured with our techniques: the DarcyPress [6] applied on small pieces of rock (10*5 mm) and the Step Decay [8] implemented on core plugs (23*25 mm). The second objective was to try to find the reasons explaining the discrepancies between the results. In order to do this, we considered many things such as: the literature, the laboratories' crushed samples as well as the data and information they accepted to share with us (raw pressure data, characteristics of the devices, experimental procedures…), the results from GRI tests we did with a device we specially designed for this study, the results from numerical simulations…

2 Study and results

2.1 Selected rocks

The three commercial laboratories which participated in the study are named Lab 1, Lab 2 and Lab 3 in the paper. Each of them received a set of samples including a piece of pyrophyllite rock, a piece of shale rock and a piece of clayey sandstone rock.

Pyrophyllite is an outcrop rock which is interesting to test methods dedicated to low permeability measurement given that it has ideal characteristics: high homogeneity, low anisotropy, low dependence on the mechanical stress and low dependence on the humidity of the ambient air. The pieces of shale rock and clayey sandstone rock were cut out from reservoir cores.

CT-scans were acquired and measurements conducted to appraise rock homogeneity and rock anisotropy. Only the reservoir cores were scanned as the pyrophyllite block was too bulky to be scanned completely. The images can be seen on Figure 2. Different layers perpendicular to the longitudinal axis are clearly identifiable on the shale core. Lamination is less visible and more discontinuous for the clayey sandstone core. The anisotropy ratio was assessed from permeability measurements for the three rocks. The results are in § 2.3.1.

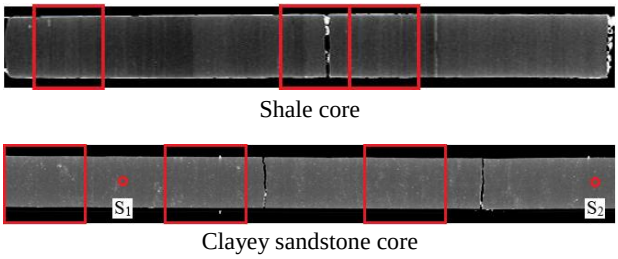

Fig. 2. CT-scans of the reservoir cores

In Table 1 are presented the values of total porosity φ_t and solid density ρ_s from the laboratories along with the values we measured. The φ_t values agree in a satisfactory manner for the three rocks. The ρ_s values are coherent for the pyrophyllite and the shale. For the clayey sandstone, our value of 2.650 $g.cm^{-3}$ diverges from the other values varying between 2.705 to 2.710 $g.cm^{-3}$. We performed a second ρ_s measurement on a sample S_2 taken far from the sample S_1 having 2.650 $g.cm^{-3}$ for ρ_s value. The samples S_1 and S_2 are located along the core on Figure 2. The new value of 2.672 $g.cm^{-3}$ was obtained. The results reveal that ρ_s is not uniform along the clayey sandstone core. This is possibly justified by local cementation knowing that the white spots disseminated over the whole scan are the core zones where the densities are the highest ones.

Table 1. ρ_s and φ_t values for the three rocks

ρ_s ($g.cm^{-3}$)				
Rock	Cyd./Tot.	Lab 1	Lab 2	Lab 3
Pyro.	2.832	2.824	2.834	2.825
Shale	2.573	2.578	2.563	2.569
Sand.	2.650	2.705	2.710	2.707
φ_t (frac)				
Rock	Cyd./Tot.	Lab 1	Lab 2	Lab 3
Pyro.	0.042	0.044	0.053	0.045
Shale	0.141	0.135	0.118	0.129
Sand.	0.044	0.035	0.033	0.040

For the pyrophyllite and the shale, the fact that the ρ_s and φ_t values are slightly dispersed tends to confirm that comparable pieces of rock were sent to the laboratories. The homogeneity of the clayey sandstone core is not easy to evaluate. On one hand, the consistency of the φ_t values would suggest that the laboratories' pieces of rock have similar permeabilities. On the other hand, the variability of the ρ_s values cast doubt upon this point.

2.2 Experimental procedures

Each laboratory received a letter of instructions with the set of three rock samples. In this letter were indicated the operations to be done on the rocks as well as the data and information needed in addition to the results and crushed samples. The experimental procedure to be followed was voluntarily simple in order that any alteration of the rock pore structure can be attributed to the crushing technique only. Notably, no solvent cleaning was demanded. Each rock had to be dried at 65 °C until mass stabilization, prior to crushing and characterization.

The letter mentioned nothing about crushing, sieving or testing to let the laboratories free to apply their standard procedures. All of them used a mechanical rock crusher and sieved the crushed materials in order to limit particle size distribution. In Table 2 are listed the specificities of the laboratories' experimental procedures.

Table 2. Characteristics of the experimental procedures

Parameter	Lab 1	Lab 2	Lab 3
Sieving			
US mesh	20/35	12/20	Not given
Testing			
T (°C)	20.5	20	20
Injected gas	Helium	Helium	Nitrogen

2.3 Crushed samples

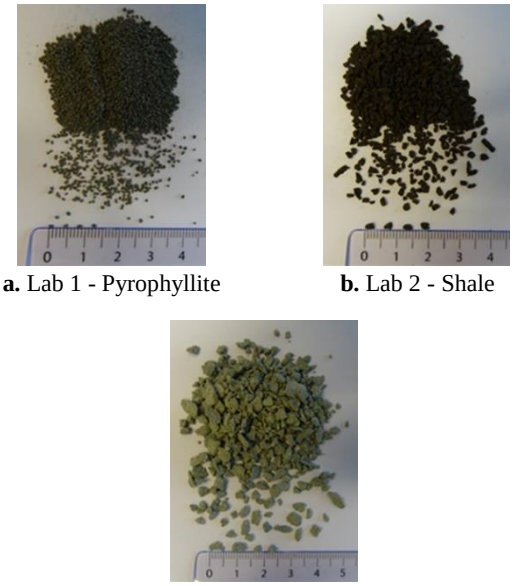

a. Lab 1 - Pyrophyllite **b.** Lab 2 - Shale

c. Lab 3 - Clayey sandstone

Fig. 3. Crushed samples

On Figure 3 are provided some photos of the laboratories' crushed samples. Unsurprisingly, the samples are packs of non-uniform rock particles. The sample from Lab 1 is visually different from the other laboratories' samples as the particles look clearly finer and more homogeneous in terms of shape and size.

The main features of the samples are in Table 3: bulk volume V_t and mean particle diameter D. The D value of 0.671 mm was not measured by Lab 1. The parameter was assumed to be equal to the mean value of the range of D values fixed by the mesh sizes chosen for sieving. Lab 2 derived D by Laser Particle Size Analysis (LPSA) on the shale crushed sample. The data are plotted on Figure 4.

Table 3. Characteristics of the crushed samples

Pyrophyllite			
Parameter	Lab 1	Lab 2	Lab 3
V_t (cm^3)	32.328	11.181	31.516
D (mm)	0.671	1.780	1.900
Shale			
Parameter	Lab 1	Lab 2	Lab 3
V_t (cm^3)	34.945	13.278	37.997
D (mm)	0.671	1.780	1.766
Clayey sandstone			
Parameter	Lab 1	Lab 2	Lab 3
V_t (cm^3)	17.971	11.450	32.705
D (mm)	0.671	1.780	1.576

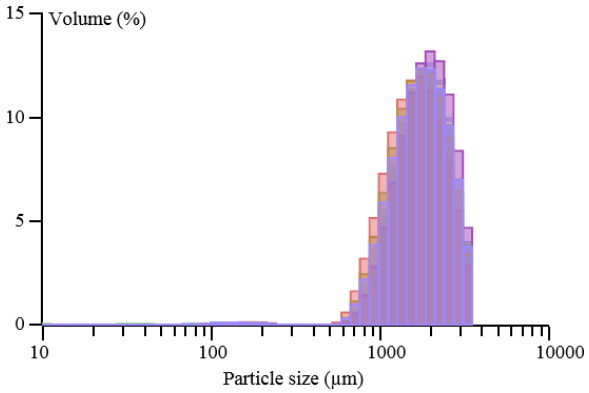

Fig. 4. Results of the LPSA for the shale

The graph reveals that the particle size distribution law is not centered on the mean value of the diameter interval. The mean D value of 1.780 mm coming from the LPSA is higher than the maximum mesh size selected by Lab 2 for sieving. This incoherence still necessitates to be clarified. Maybe sieving was not as efficient as expected owing to the irregular particle shapes. One can easily imagine that the particles will hardly be held back by the sieve screens if they are elongated.

V_t and D are both inputs of the interpretative model. V_t is as complicated as D to estimate, notably in the case where the laboratory receives cuttings or a sample already crushed [9]. How do the uncertainties on these parameters affect the results coming from the interpretation? A huge work would be needed to answer this question.

2.3 Permeability results

2.3.1 k_l and b values from Cydarex and Total

For the three rocks, we measured the absolute or intrinsic permeability k_l and the Klinkenberg coefficient b, by Step Decay [8] for Total and DarcyPress [6] for Cydarex.

The orientation of the bedding plane was obvious for the reservoir cores but not for the pyrophyllite block. This is the reason why the sampling directions are identified, in the paper, in relation to the space directions (numbered from 1 to 3) for the pyrophyllite and to the bedding plane for the shale and the clayey sandstone. We will talk about sampling parallel (//) or perpendicular (⊥) to bedding for the reservoir cores. We supposed that the rock properties are equivalent in the two directions parallel to bedding.

Total performed the tests on plugs having a diameter of 23 mm and a length of 25 mm, injecting nitrogen only. Four plugs were taken from the pyrophyllite block. One plug was sampled in each space direction to orientate and quantify the anisotropy. A last plug was sampled far from the three others to check the homogeneity. The results are reported in Table 4. They were determined at an effective confining pressure P_{eff} of around 80 barg. The plugs were not dried before analysis because the pyrophyllite proved to be quite insensitive to the humidity of the ambient air. The results demonstrate that the rock is homogeneous and slightly anisotropic, the anisotropy ratio reaching about a factor of 2. The k_l value in Direction 2 is the lowest one and the k_l values in Direction 1 and Direction 3 are very close. When the study was started, all the unconventional reservoir cores stored at Total's core house were no longer cylinders but half-cylinders. Plug sampling perpendicular to bedding was not feasible, as a consequence. Sampling parallel to bedding was problematic too knowing that the volume of rock available per facies was small according to the laboratories' needs. In the end, only one plug could be taken per reservoir core, parallel to bedding. The data are also in Table 4. Those corresponding to the shale plug were not validated since CT-scans evidenced fractures in the plug. The test on the clayey sandstone was conducted at a low P_{eff} value of around 60 barg to limit the effect of the confinement on the permeability. Prior to testing, the plug was dried in an oven at 65 °C until mass stabilization, to respect the instructions passed on to the laboratories.

Table 4. k_l and b values measured by Total

Pyrophyllite			
23*25 mm cylinders - Nitrogen - $P_{eff} \approx 80$ barg			
Plug	Direction	k_l (nD)	b (bara)
1	1	55	31
2	2	28	31
3	3	58	30
4	1	61	29
Clayey sandstone			
23*25 mm cylinder - Nitrogen - $P_{eff} \approx 60$ barg			
Plug	Direction	k_l (nD)	b (bara)
S_1 (§ 2.1)	// to bedding	19	21

Cydarex prepared for the tests small rock cylinders of 10 mm of diameter and 5 mm of length embedded in resin discs of 25 mm of diameter and 5 mm of length. Sampling was undertaken in Direction 2 and in Direction 3 for the pyrophyllite, parallel and perpendicular to bedding for the reservoir rocks. The results are in Table 5. The tests were run at an axial confining pressure P_{axial} of about 100 barg, with nitrogen for the three rocks and with helium as well for the reservoir rocks. The samples were dried at 65 °C until mass stabilization. Total received from Cydarex two DarcyPress samples for characterization by Step Decay. The cylinders of shale and clayey sandstone were taken perpendicular to bedding. The diameter of the resin discs was reduced from 25 to 23 mm so that the samples fit in the core holder of the Step Decay device. The results are in Table 5 again. The tests were conducted with nitrogen, at a P_{eff} value of about 60 barg.

Table 5. k_l and b values measured by Cydarex and Total

Cydarex - Pyrophyllite			
10*5 mm cylinders - Nitrogen - $P_{axial} \approx 100$ barg			
Sample	Direction	k_l (nD)	b (bara)
1	2	32	32
2	3		
Cydarex - Shale			
10*5 mm cylinders - Nitrogen - $P_{axial} \approx 100$ barg			
Sample	Direction	k_l (nD)	b (bara)
1	// to bedding	28	18
2	⊥ to bedding	8	28
Total - Shale			
10*5 mm cylinders - Nitrogen - $P_{eff} \approx 60$ barg			
Sample	Direction	k_l (nD)	b (bara)
3	⊥ to bedding	6	7
Cydarex - Shale			
10*5 mm cylinders - Helium - $P_{axial} \approx 100$ barg			
Sample	Direction	k_l (nD)	b (bara)
1	// to bedding	24	61
2	⊥ to bedding	11	51
Cydarex - Clayey sandstone			
10*5 mm cylinders - Nitrogen - $P_{axial} \approx 100$ barg			
Sample	Direction	k_l (nD)	b (bara)
1	// to bedding	4	13
2	⊥ to bedding		
Total - Clayey sandstone			
10*5 mm cylinders - Nitrogen - $P_{eff} \approx 60$ barg			
Sample	Direction	k_l (nD)	b (bara)
3	⊥ to bedding	0.8	41
Cydarex - Clayey sandstone			
10*5 mm cylinders - Helium - $P_{axial} \approx 100$ barg			
Sample	Direction	k_l (nD)	b (bara)
1	// to bedding	4	28
2	⊥ to bedding		

When two lines are merged in Table 5, it means that Sample 1 and Sample 2 have comparable k_l or b values. In other words, the discrepancies were too low compared to the uncertainties so that one value can be differentiated from the other.

For the pyrophyllite, there is a satisfactory agreement between the values of k_l derived for the 23*25 mm plugs by Total and those determined for the 10*5 mm plugs by Cydarex. The same observation applies to the b values.

The data collected for the small shale plugs highlight that: (i) The k_l values from tests run on different samples and with different methods are coherent, contrary to the b values. (ii) The k_l values obtained with different gases are coherent. (iii) The shale rock has an anisotropy ratio of 3 approximately. (iv) The ratio of the b value measured with helium to the b value measured with nitrogen is not so far from the expected value of 2.9, parallel and perpendicular to bedding. The theoretical value of 2.9 was computed by applying the following relationship:

$$\frac{b_{helium}}{b_{nitrogen}} = \frac{\mu_{helium}}{\sqrt{M_{helium}}} \frac{\sqrt{M_{nitrogen}}}{\mu_{nitrogen}} \quad (1)$$

The expression of b, true for any gas, was drawn from the reference [10]:

$$b = \frac{4c\mu}{r}\sqrt{\frac{\pi RT}{M}} \quad (2)$$

In Equation (1), M is the gas molecular weight and μ the gas viscosity. In Equation (2), c is a coefficient close to 1, r is the radius in mm of the capillary tubes used to model the pore network and R is the universal gas law constant.

For the clayey sandstone, the precedent remarks made for the shale change as follows: (i) The k_l values from tests involving different samples and methods are not coherent, as well as the b values. (ii) The k_l values estimated with different gases are similar. (iii) The sandstone rock has a negligible anisotropy ratio. (iv) The ratio of b is close to 2.9.

To sum up, the DarcyPress and Step Decay k_l values converge for the pyrophyllite and the shale while, for the clayey sandstone, discrepancies reaching until a factor of 5 were noted. Regarding our b values, they are consistent for the pyrophyllite only. The discrepancies range from a factor of 1.6 to a factor of 3, for the shale and the clayey sandstone. Finding the reasons why the k_l and/or b values are dispersed for the reservoir cores would be a complex task. Lack of representativity of the small samples due to the heterogeneity of the rocks at small scale? Anisotropy? Multiplicity of the methods and experimental conditions? More tests would be needed to answer these questions.

2.3.2 k_{app} values from the commercial laboratories

Values of apparent permeability k_{app} were collected from the three commercial laboratories although k_l values were demanded in the letter of instructions. Graphs of apparent permeability k_{app} plotted against the inverse of the mean pore pressure P_m were built to enable the comparison of our results to the laboratories' results. They are shown on Figure 5, Figure 6 and Figure 7. Two graphs are given per type of rock, the first one for nitrogen and the second one for helium. On each graph is delimited the area covering the possible k_{app} values expected for the rock and the gas considered, when neglecting the effect of the confinement on k_{app}. The upper and lower limit lines were drawn using Klinkenberg law [10]:

$$k_{app} = k_l\left(1 + \frac{b}{P_m}\right) \quad (3)$$

Notably, every potential lower or upper limit was plotted to have the maximal area in which the laboratories' k_{app} values should lie, according to all of our pairs of k_l and b values. The lower limits are based on the pairs of values associated to the least permeable samples. These samples are those taken parallel to Direction 2 for the pyrophyllite and perpendicular to bedding for the reservoir rocks. On the opposite, the upper limits rely on the pairs of values corresponding to the most permeable samples, which are parallel to Direction 3 for the pyrophyllite and parallel to bedding for the reservoir rocks. When no tests were done with helium on the samples characterized with nitrogen, the limits were plotted on the graph for helium with the k_l values for nitrogen and b values equal to 2.9 times those for nitrogen.

The notations "D." and "D.s" appearing in the legends of the graphs of Figure 5, Figure 6 and Figure 7 stand for "Direction" and "Directions" respectively.

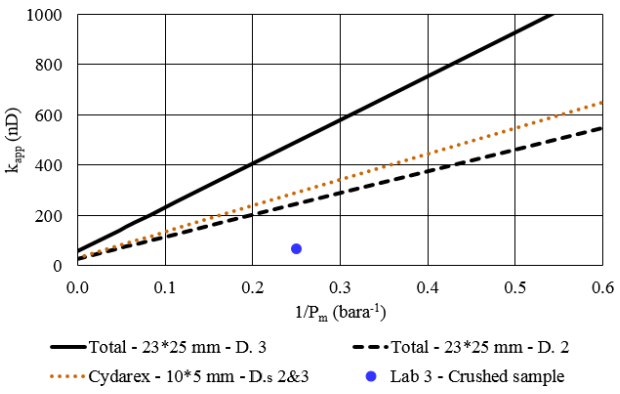

a. Nitrogen

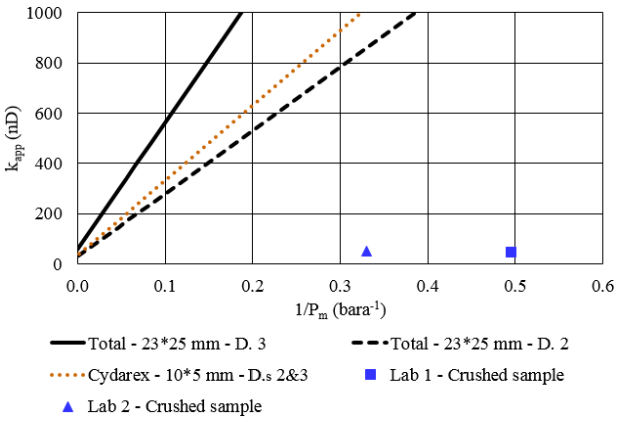

b. Helium

Fig. 5. $k_{app} = f(1/P_m)$ graph for the pyrophyllite

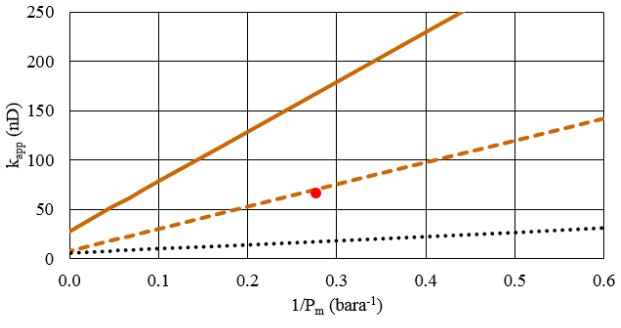

a. Nitrogen

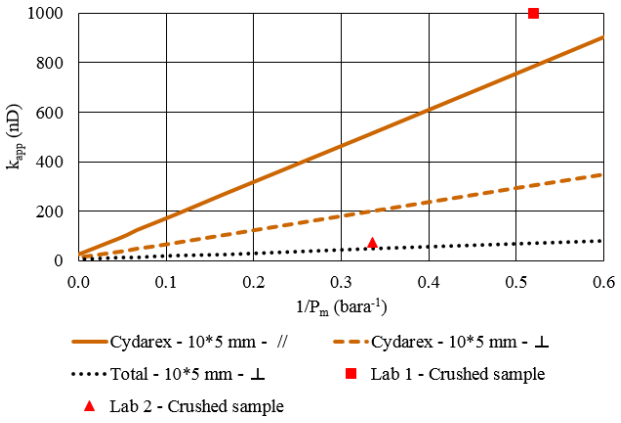

b. Helium

Fig. 6. $k_{app} = f(1/P_m)$ graph for the shale

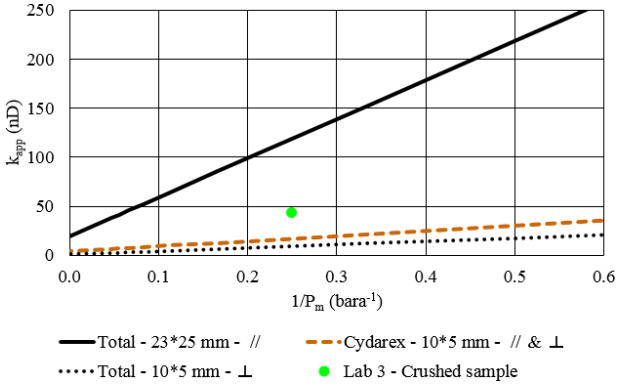

a. Nitrogen

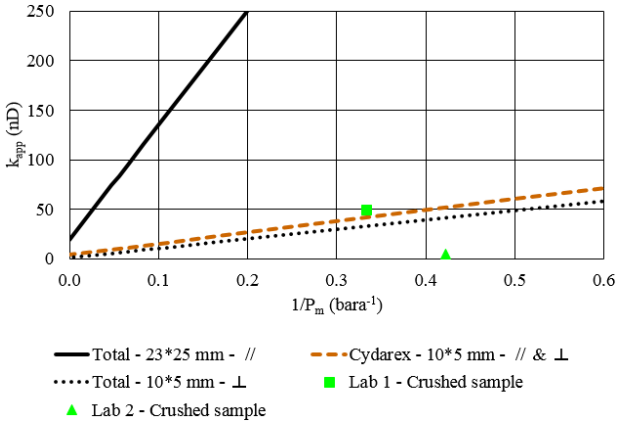

b. Helium

Fig. 7. $k_{app} = f(1/P_m)$ graph for the clayey sandstone

The k_{app} values from the laboratories were reported on the graphs by associating them to the P_m values computed from Equation (4). P_2 is the initial absolute pressure in the rock particles and $P_{f,1+2}$, the final one.

$$P_m = \frac{P_2 + P_{f,1+2}}{2} \qquad (4)$$

It must be noted that the value deduced from Equation (4) is an approximation. In a classical steady-state test, P_m is the mean pore pressure recorded at steady-state. In a GRI test where no steady-state regime is reached, what is the P_m value to be assigned to the k_{app} value? This question is not easy to answer. At least, P_m cannot be taken equal to the mean pressure recorded at the surface of the particles.

Less than 50 % of the laboratories' k_{app} values are in the areas of expected values. Hence, working on crushed samples generates even more dispersion in the values of permeability. The k_{app} values tend to be at the bottom of the areas or to be below their lower limits. Discrepancies from a factor of 3.5 to a factor of 28 can be noted between the measured k_{app} values and the lowest predicted values.

One argument extracted from the literature [1] which could explain the observations is that crushing eliminated the micro-fractures whereas such fractures were present in the DarcyPress and Step Decay samples. Given that the highest discrepancies were observed for the pyrophyllite, this rock was selected for SEM imaging at plug scale and at particle scale. The rock particles came from the crushed samples prepared by the three laboratories. The images of Figure 8 reveal the existence of fractures in some particles but not in the piece of plug. This piece of plug seems to be more intact than the particles, which goes against the argument drawn from the reference [1].

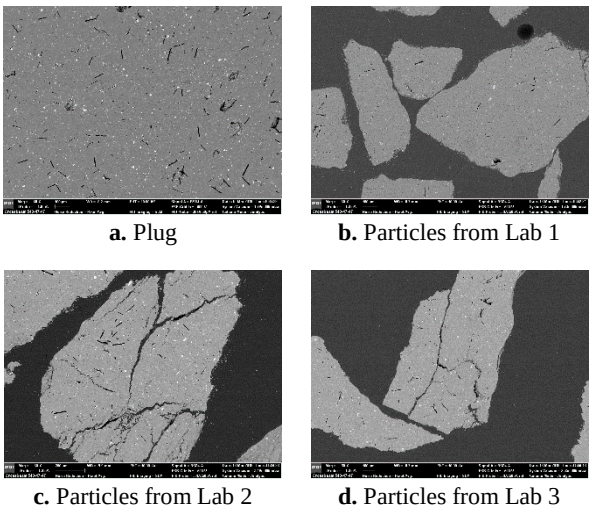

a. Plug **b.** Particles from Lab 1

c. Particles from Lab 2 **d.** Particles from Lab 3

Fig. 8. SEM images on plug and particles for the pyrophyllite

2.4 Experimental devices

While Lab 1 and Lab 2 worked with experimental devices similar to the GRI device represented on Figure 1, Lab 3 developed a different device by removing the chamber V_1 and connecting the valve v_{1-2} to the gas source. The valve opens for a fraction of second at the beginning of the test

in order that the pressure pulse is directly produced in the dead volume of the chamber V_2. The initial pressure at the surface of the particles is better controlled in this way. The three laboratories reduced at maximum the dead volume around the crushed sample by placing calibrated billets in the chamber V_2. In Table 6 are detailed the specificities of the laboratories' devices. DV designates the dead volume remaining in the chamber V_2 after filling with the sample and the billets.

Table 6. Characteristics of the devices

Pyrophyllite			
Volume	Lab 1	Lab 2	Lab 3
V_1 (cm^3)	24.985	59.381	-
V_2 (cm^3)	144.382	67.754	105.510
$V_{billets}$ (cm^3)	57.617	30.667	38.220
DV (cm^3)	54.437	25.906	35.774
Shale			
Volume	Lab 1	Lab 2	Lab 3
V_1 (cm^3)	24.985	59.381	-
V_2 (cm^3)	144.382	67.754	106.810
$V_{billets}$ (cm^3)	54.043	27.451	41.090
DV (cm^3)	55.394	27.025	27.723
Clayey sandstone			
Volume	Lab 1	Lab 2	Lab 3
V_1 (cm^3)	24.985	59.381	-
V_2 (cm^3)	144.382	67.754	105.510
$V_{billets}$ (cm^3)	82.722	29.045	35.280
DV (cm^3)	43.689	27.259	37.525

2.5 Experimental signals

Figure 9 shows the laboratories' raw pressure signals.

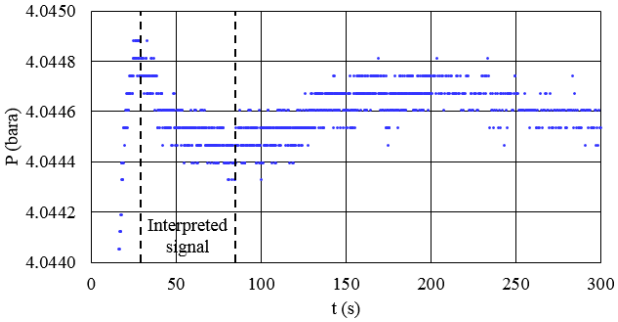

a. Pyrophyllite - Lab 1

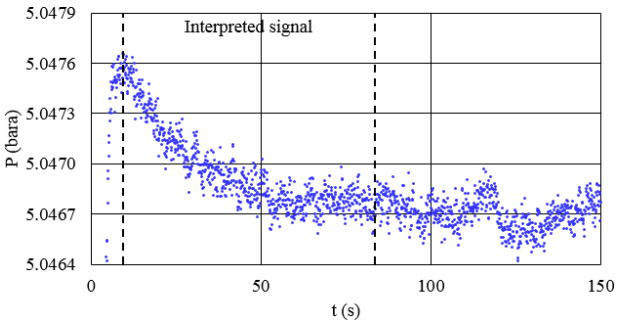

b. Pyrophyllite - Lab 2

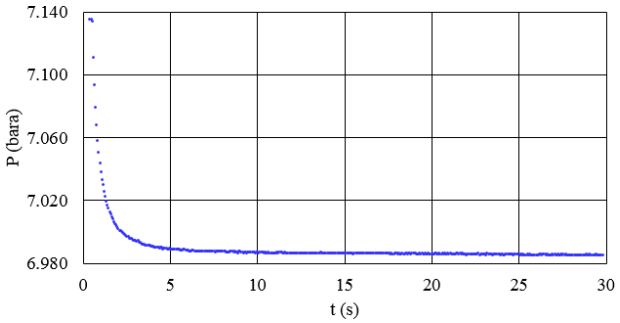

c. Pyrophyllite - Lab 3

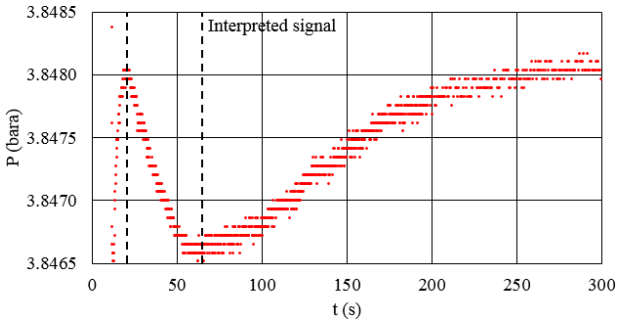

d. Shale - Lab 1

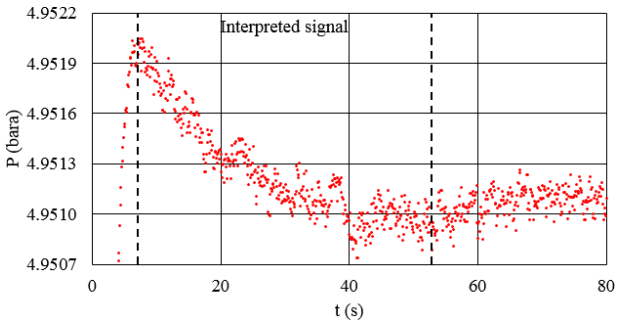

e. Shale - Lab 2

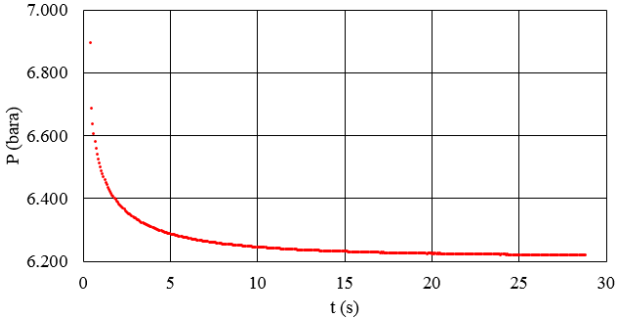

f. Shale - Lab 3

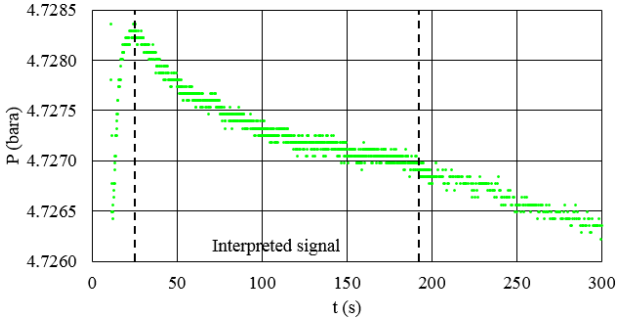

g. Clayey sandstone - Lab 1

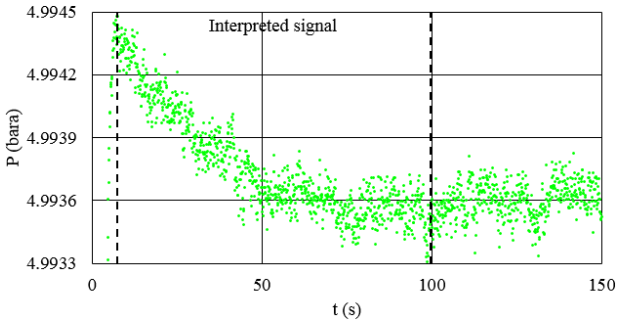

h. Clayey sandstone - Lab 2

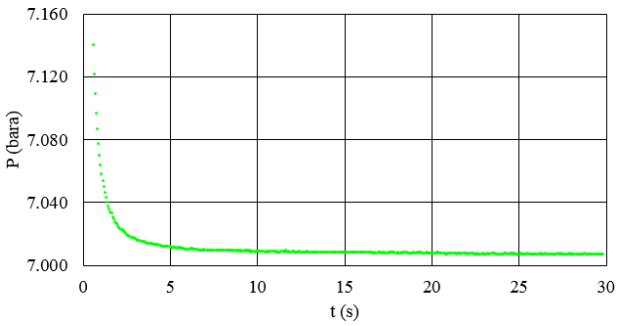

i. Clayey sandstone - Lab 3

Fig. 9. Pressure signals

The signals tend to be short and noisy, short because of the small particle sizes and noisy because of the small pressure variations due to the small sample pore volumes. The signal durations range from about 1 to 150 s and the signal amplitudes from less than 1 mbar to a few hundreds of millibar, according to the data in Table 7.

Table 7. Characteristics of the pressure signals

Pyrophyllite			
Parameter	Lab 1	Lab 2	Lab 3
P_1 (bara)	13.103	6.853	-
P_2 (bara)	0	Ambient	Ambient
$P_{i,1+2}$ (bara)	4.0449	5.0477	7.1353
$P_{f,1+2}$ (bara)	4.0445	5.0467	6.9856
θ (mbar)	0.414	0.737	149.628
Δt (s)	≈ 50	≈ 100	≈ 15
Shale			
Parameter	Lab 1	Lab 2	Lab 3
P_1 (bara)	13.108	6.854	-
P_2 (bara)	0	Ambient	Ambient
$P_{i,1+2}$ (bara)	3.8480	4.9520	6.8965
$P_{f,1+2}$ (bara)	3.8466	4.9511	6.2197
θ (mbar)	1.379	0.869	676.802
Δt (s)	≈ 50	≈ 50	≈ 30
Clayey sandstone			
Parameter	Lab 1	Lab 2	Lab 3
P_1 (bara)	13.121	6.853	-
P_2 (bara)	0	Ambient	Ambient
$P_{i,1+2}$ (bara)	4.7284	4.9945	7.1605
$P_{f,1+2}$ (bara)	4.7270	4.9935	7.0075
θ (mbar)	1.379	0.971	152.990
Δt (s)	≈ 150	≈ 100	≈ 15

Regarding the notations in Table 7, $P_{i,1+2}$ is the initial pressure recorded just after opening the valve v_{1-2} in the chamber V_1 and in the dead volume DV of the chamber V_2 while $P_{f,1+2}$ is the equilibrium pressure in the system at the end of the test. Furthermore, θ and Δt are respectively the amplitude and the duration of the pressure signal. The θ value in Table 7 is an approximate value, the pressure $P_{i,1+2}$ being affected by an error generated by the thermal effect produced at the opening of the valve v_{1-2}.

The quality of the pressure signals varies depending on the laboratory. Because of their very low amplitudes, the signals from Lab 1 suffer from the lack of resolution of the pressure sensor while those from Lab 2 suffer more from the noise affecting pressure acquisition. Resolution and noise do not impact as much the signals from Lab 3, the errors they engender being relatively low compared to the pressure variations. In other words, the good quality of the signals from Lab 3 is due to their high amplitudes. These high amplitudes are themselves related to the high amounts of crushed materials considered for the tests and to the limited volume (namely, the dead volume DV of the chamber V_2, no chamber V_1 being used) depleted during the gas flow in the sample pore volume.

For any type of rock, the pressure signal from Lab 3 is systematically the shortest one. This is not coherent with the fact that the particle sizes chosen by Lab 1 and Lab 2 are smaller or comparable to those chosen by Lab 3. This is also not coherent with the fact that Lab 3 worked with nitrogen while Lab 1 and Lab 2 injected helium. Indeed, the pressure signal is expected to be shorter with helium since the lower the gas molar mass, the higher b and thus, the higher k_{app}. The signals from Lab 1 and Lab 2 never stabilize, contrary to those from Lab 3. This suggests that they could be impacted by experimental artifacts, thermal effects or something completely different? It is difficult to identify the causes of this behavior.

2.6 Interpretative models

Only Lab 3 accepted to reveal information regarding the model used to interpret the GRI tests. The crushed sample was assimilated to a monodisperse pack of homogeneous and isotropic spheres. Moreover, the gas was supposed to be ideal, to have a constant viscosity and to propagate in isothermal conditions. Lab 3 solved the physical problem analytically and in Laplace space. The gas compressibility was assumed to be independent of pressure in order that a solution can be computed. This solution is at the center of the interpretative procedure implemented to estimate k_{app} by history matching the simulated pressure signal with the recorded pressure signal. It is inverted numerically using Stehfest algorithm to be given in time space.

3 Discussion

3.1 GRI tests by Cydarex and Total

3.1.1 Device, sample, procedure and interpretation

To better understand the limits of the GRI technique, we developed our own device for permeability measurement on crushed rock. Our device is similar to that sketched on Figure 1. The test is run following the standard procedure described in the introduction but with the material in the chamber V_1. The response recorded after opening of the valve $v_{1\text{-}2}$ is no longer a pressure decay. It increases over time while the gas flows out from the medium. Figure 10 shows an example of experimental signal obtained with our device on a pyrophyllite crushed sample.

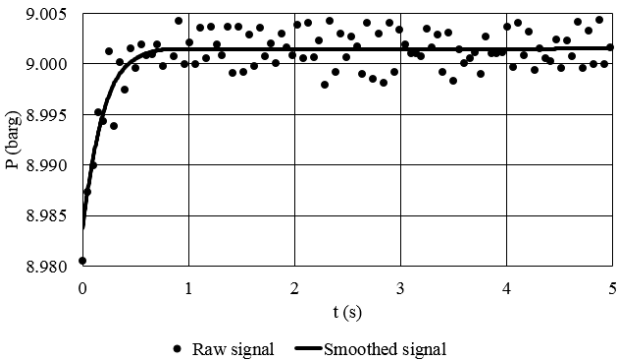

Fig. 10. Example of recorded and smoothed pressure signals

The signal is noisy owing to small pressure variations but it properly stabilizes at long times. A meticulous work aiming at reducing as much as possible the experimental and thermal artifacts was done over the whole prototype elaboration phase. This work was essential to ensure the reliability of the small recorded signals. The noise is not so problematic knowing that it can be eliminated with an appropriate signal processing method. Such a method was systematically implemented to smooth the signal prior to interpretation. An example of smoothed signal appears on Figure 10.

The model intervening in the interpretative procedure is based on two hypotheses. First, the crushed sample is assumed to be a monodisperse pack of homogeneous and isotropic spheres. Second, the gas is supposed to be ideal, to have a constant viscosity and to propagate in isothermal conditions. The model is a numerical model which takes into account the gas compressibility. It is at the center of a history matching procedure providing an estimation of k_{app} at the end of the interpretation. Determining k_l and b values instead of a k_{app} value would not be feasible as the two properties are correlated [2]. The approach adopted to discriminate k_l from b was to conduct tests at increasing P_m values and to deduce k_l and b from the coefficients of the linear regression on the points of k_{app} plotted against $1/P_m$. Refer to § 2.3.2 for the comments about the P_m value to be assigned to the k_{app} value. Figure 11 is an example of $k_{app} = f(1/P_m)$ graph for a shale crushed sample.

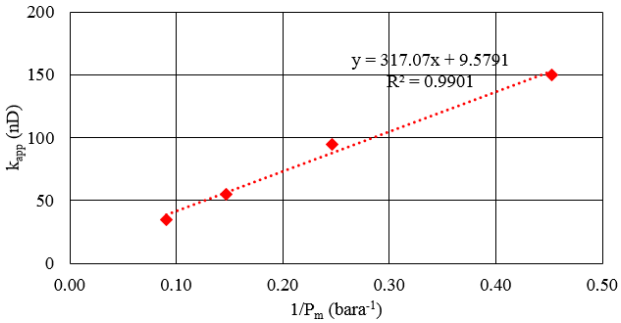

Fig. 11. $k_{app} = f(1/P_m)$ graph for the shale

3.1.2 Validity domain

As previously mentioned in the introduction, the pressure signal is impacted by thermal effects at early times. These effects were not introduced in the interpretative model. It is then obvious that the signal due to the gas flow out from the sample must be more significant than the signal due to the thermal perturbations so that the estimated k_{app} value can be validated. The period over which errors affect the recorded pressures when injecting nitrogen was assessed experimentally. A highly permeable material called BLM was chosen for the tests. Its k_l value is equal to 7 mD. For such a k_l value and a mean particle diameter of 1.720 mm, the pressure signal related to the gas flow in the sample pore network vanishes quite instantaneously. This means that the entire recorded signal can be attributed to thermal effects. The signal acquired for BLM with nitrogen is on Figure 12.

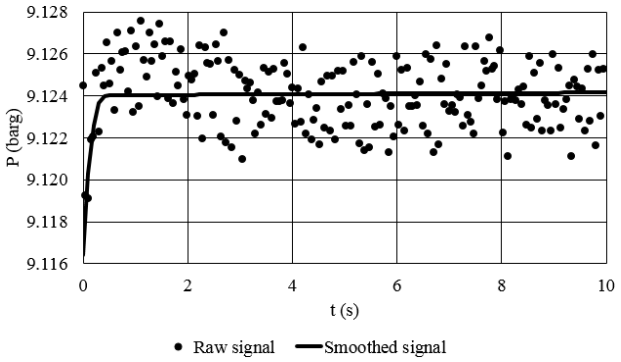

Fig. 12. Pressure signal recorded for BLM with nitrogen

The signal persists approximately 0.5 s. This duration was taken as a criterion to propose a graph of k_{app} plotted against φ_t where is delimited, in a specific experimental configuration, the validity domain of the GRI technique applied with our device. Figure 13 is an example of such a graph, where the validity domain is delimited for three mean particle sizes. The graph was built from numerical simulations undertaken with the parameters defining the experimental configuration adopted for the tests tackled in § 3.1.3. For a given D value, the couples of φ_t and k_{app} values lying on the associated curve ensure the recording of a pressure signal which is long enough compared to that acquired for BLM. A test is validated when the (φ_t, k_{app}) couple is below the curve and disregarded in the opposite case.

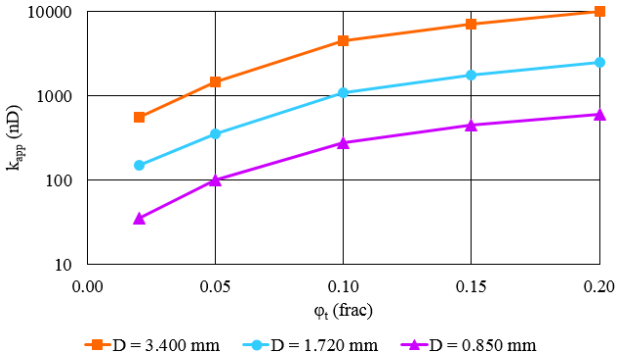

Fig. 13. $k_{app} = f(\varphi_t)$ graph for nitrogen

3.1.3 Results

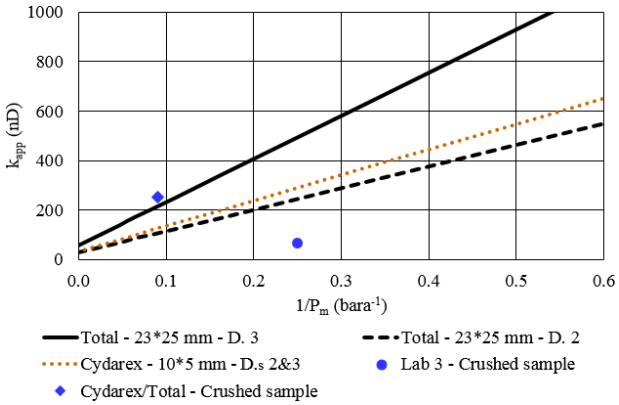

Fig. 14. $k_{app} = f(1/P_m)$ graph for the pyrophyllite

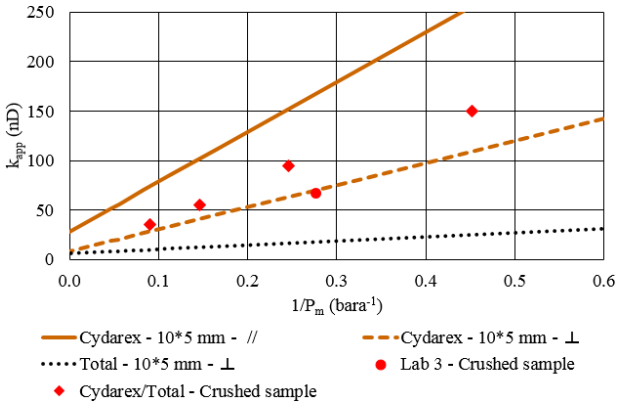

Fig. 15. $k_{app} = f(1/P_m)$ graph for the shale

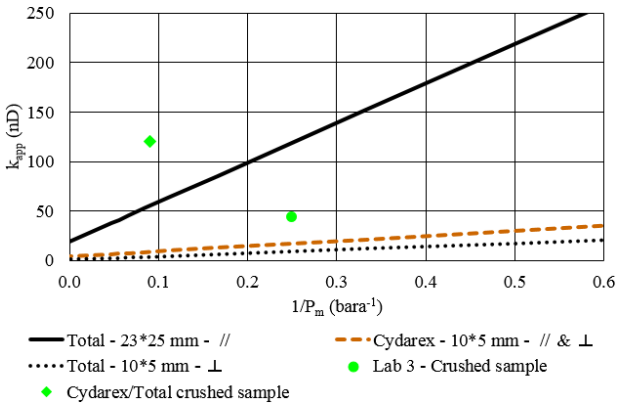

Fig. 16. $k_{app} = f(1/P_m)$ graph for the clayey sandstone

We carried out GRI tests on one crushed sample of each type of rock injecting nitrogen. The graphs for nitrogen of Figure 5 to Figure 7 were completed with our k_{app} values. The new graphs are those of Figure 14 to Figure 16.

Our k_{app} values lie in the predicted area for the shale and a bit above the upper limit for the pyrophyllite. The k_{app} value for the clayey sandstone is quite equal to twice the upper limit value. Paying attention to eliminate at best the experimental and thermal artifacts altering the signal quality probably contributed to decrease the dispersion of the results. For the pyrophyllite and the clayey sandstone, one could think that the higher than expected k_{app} values are maybe due to a problem of validity of the tests. This justification would not be absurd, both rocks being poorly porous and then bad candidates to acquire long signals. However, the graph of Figure 17 highlights that, as well as the (φ_t, k_{app}) couples for the shale, the couples for the pyrophyllite and the clayey sandstone are in the validity domain of the method.

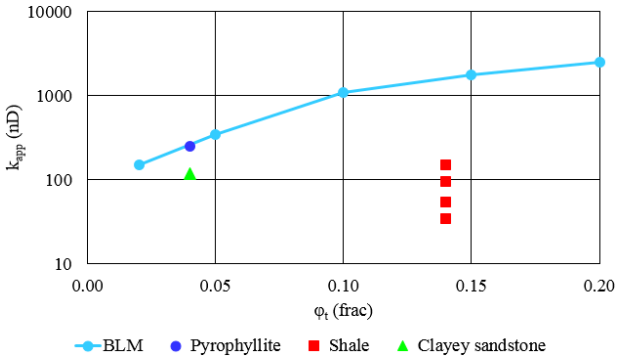

Fig. 17. Cydarex/Total results on $k_{app} = f(\varphi_t)$ graph for nitrogen and D = 1.720 mm

3.2 Cydarex/ Total model versus laboratories' models

As the laboratories sent all of the parameters concerning their samples and devices, it was possible to predict with our model the pressure signal expected from a GRI test in a specific experimental configuration and for specific k_l and b values. The exercise was done for the pyrophyllite, using the parameters coming from Lab 2. On the graph of Figure 18, the signal recorded by Lab 2 when testing the pyrophyllite crushed sample with helium is compared to two numerical signals. The first one was simulated with the k_l and b values from Total and, more exactly, with the k_l value for nitrogen and the b value for nitrogen increased by a factor of 2.9. The second one was simulated with the k_{app} value from Lab 2. There is no coherence between the experimental and numerical signals. It is not surprising to see that the recorded signal does not match with the signal simulated from Total's k_l and b values since the existence of discrepancies between the laboratories' results and our results is known. It is more problematic to notice that the signal simulated with the k_{app} value from Lab 2 is faster than the recorded signal. This suggests that Lab 2 works with a model differing from ours.

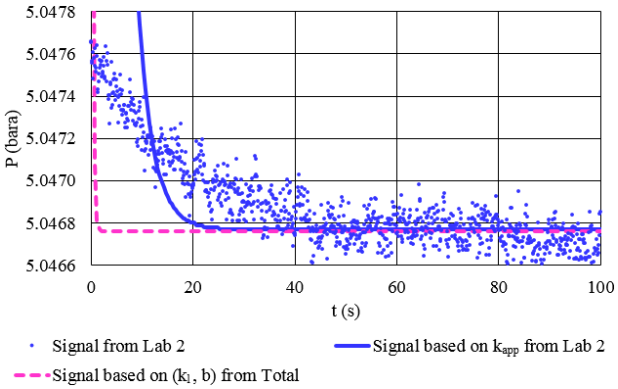

Fig. 18. Recorded signal versus simulated signals

4 Conclusions

Reconciling permeability data determined on samples of different sizes and by different laboratories having their own methods and experimental procedures is challenging. This is illustrated in the present paper for three materials: one homogeneous and slightly anisotropic outcrop rock named pyrophyllite and two reservoir rocks which were fairly homogeneous and moderately anisotropic.

The study started with the comparison of our methods dedicated to low permeability measurement: DarcyPress for small cylinders (10*5 mm) and Step Decay for bigger cylinders (23*25 mm). Consistency was noticed between the k_l values as between the b values for the pyrophyllite only. For the reservoir cores, the results were dispersed. The discrepancies reached at maximum a factor of 5 for k_l and a factor of 3 for b.

Three commercial laboratories having their own GRI techniques were contacted to characterize the three rocks following their standard procedures. The crushed samples they prepared were made up with particles having mean diameters between 0.7 and 1.9 mm. The three laboratories provided k_{app} values instead of the demanded k_l values. A range of possible k_{app} values was hence defined for each rock from the k_l and b values we estimated. About 50 % of the delivered k_{app} values were in the predicted ranges and rather close to the lowest limits. The remaining k_{app} values were mostly lower than the lowest expected values. Discrepancies ranging from a factor of 3.5 to a factor of 28 were noted. The k_{app} values from the GRI tests created hence more dispersion in the permeability data. The fact that the k_{app} values for the crushed samples tend to be low is not justified by the elimination of microfractures during crushing. Indeed, SEM images done for the pyrophyllite showed fractures in some particles of the crushed samples but not in the plug. Crushing seems to damage the rock.

The comparison of the permeabilities drawn from the Step Decay, DarcyPress and GRI tests evidenced that the dispersion of the results increases when the characteristic length of the medium decreases. Thus, one of the reasons explaining why many laboratories' k_{app} values are out of the ranges of expected values would be the heterogeneity of the materials at small scale. This means that the crushed samples are potentially not representative of the rocks. A second reason could be the bad quality of the raw pressure signals. For two laboratories out of three, the signals were clearly affected by experimental or thermal artifacts since they were long and not stabilized at equilibrium. The third laboratory acquired signals having good amplitudes and durations by acting simultaneously on the sample features and on the device design. A third possible reason would be the diversity of the laboratories' interpretative models and the difficulty to define some input parameters such as the mean particle size for instance. A crushed sample is a complex system to model. The impacts of the simplifying assumptions made when building the model are generally hard to appraise.

We developed a GRI device especially for the study and we performed tests with it on the pyrophyllite and on the reservoir rocks. We spent time to eliminate at best the experimental and thermal artifacts impacting the pressure signal. This was indispensable to ensure the reliability of the recorded pressure values. Besides, we carried out tests on a highly permeable rock to identify the minimal signal duration needed with our device to ensure the validity of the test and of the results. The derivation of k_l and b values from several tests run at increasing mean pore pressures proved to be satisfactory. Moreover, our k_{app} values were closer to the expected values than the k_{app} values from the laboratories. Being careful to the signal quality probably contributed to decrease the dispersion of the permeability data.

We do not pretend that our results are more accurate than those provided by the commercial laboratories. It is hard to know if the discrepancies are due to experimental issues, the interpretative models or the representativity of the samples. We believe that it is essential to continue the analysis of the GRI method and launch other benchmarks before considering it as a "routine" laboratory method. If we refer to the study of the centrifuge method historically initiated by the SCA [11], it could be fruitful to compare the numerical models used for interpretation on synthetic data.

References

1. D. L. Luffel, C. W. Hopkins and P. D. Shettler, "Matrix permeability measurement of gas productive shales", presented at the 68th SPE Annu. Tech. Conf. and Exhibition, Houston, TX, USA, Oct. 3 - 6, 1993, Paper SPE 26633.
2. S. Profice, D. Lasseux, Y. Jannot, N. Jebara and G. Hamon, "Permeability, porosity and Klinkenberg coefficient determination on crushed porous media", *Petrophysics*, vol. 53, n° 06, Dec. 2012.
3. O. Kwon, A. K. Kronenberg, A. F. Gangi and B. Johnson, "Permeability of Wilcox shale and its effective pressure law", *J. Geophys. Res.*, vol. 106, n° B9, pp. 19,339 - 19,353, Sep. 10, 2001.

4. Q. R. Passey, K. M. Bohacs, W. L. Esch, R. Klimentidis and S. Sinah, “From oil-prone source rock to gas-producing shale reservoir - Geologic and petrophysical characterization of unconventional shale-gas reservoirs”, presented at the CPS/SPE Int. Oil & Gas Conf. and Exhibition, Beijing, China, Jun. 8 - 10, 2010, Paper SPE 131350.
5. A. Tinni, E. Fathi, R. Agarwal, C. H. Sondergeld, I. Y. Akkutlu and C. S. Rai, “Shale permeability measurements on plugs and crushed samples”, presented at the SPE Canadian Unconventional Resources Conf., Calgary, AB, Canada, Oct. 30 - Nov. 1, 2012, Paper SPE 162235.
6. R. Lenormand, F. Bauget and G. Ringot, “Permeability measurement on small rock samples”, presented at the SCA Int. Symp., Halifax, NS, Canada, Oct. 04 - 07, 2010, Paper SCA2010-32.
7. P. Egermann, R. Lenormand, D. Longeron and C. Zarcone, “A fast and direct method of permeability measurements on drill cuttings”, *Petrophysics*, vol. 44, n° 4, pp. 243 - 252, Jul. - Aug. 2003.
8. D. Lasseux, Y. Jannot, S. Profice, M. Mallet and G. Hamon, “The “Step Decay”: a new transient method for the simultaneous determination of intrinsic permeability, Klinkenberg coefficient and porosity on very tight rocks”, presented at the SCA Int. Symp., Aberdeen, Scotland, Aug. 27 - 30, 2012, Paper SCA2012-25.
9. R. Lenormand and O. Fonta, “Advances in measuring porosity and permeability from drill cuttings”, presented at the SPE/EAGE Reservoir Characterization and Simulation Conf., Abu Dhabi, U. A. E., Oct. 28 - 31, 2007, Paper SPE 111286.
10. L. J. Klinkenberg, “The permeability of porous media to liquids and gases”, *Drilling and Production Practice*, pp. 200 - 213, Jan. 1, 1941.
11. P. Forbes, “Centrifuge data analysis techniques: a SCA survey on the calculation of drainage capillary pressure curves from centrifuge measurements”, presented at the SCA Int. Symp., Calgary, AB, Canada, Sep. 8 - 10, 1997, Paper SCA-9714.

Nomenclature

b	Pa	Klinkenberg coefficient
c	-	Coefficient close to 1
D	m / -	Diameter / Direction
DV	-	Dead volume
k	m^2	Permeability
M	$g.mol^{-1}$	Molecular weight
P	Pa	Pressure
r	m	Radius
R	$J.mol^{-1}.K^{-1}$	Universal gas law constant
S	-	Sample
t	s	Time
T	K	Temperature
v	-	Valve
V	m^3	Volume
Δt	s	Duration
θ	Pa	Amplitude
μ	Pa.s	Viscosity
ρ	$kg.m^{-3}$	Density
φ	-	Porosity
//	-	Parallel
$\perp$	-	Perpendicular

Subscripts

app	-	Apparent
eff	-	Effective
f	-	Final
i	-	Initial
l	-	Absolute
m	-	Mean
s	-	Solid
t	-	Total / Bulk